Capture Gamma-Ray Studies

H. E. KUBITSCHEK AND S. M. DANCOFF
Physics Department, University of Illinois, Urbana, Illinois and Argonne National Laboratory, Chicago, Illinois
(Received April 12, 1949)

Measurements are made of the maximum energies of gamma-rays emitted on neutron capture by a number of elements. Values so obtained are in rough agreement with semi-empirical formulas for neutron binding energies. Evidence is presented to show that gamma-rays carrying nearly the maximum energy are observed much more frequently than would be expected on statistical theories. The yield of gamma-rays on neutron capture is studied and found to show a variation, on the elements examined, of ±30 percent about a mean.

INTRODUCTION

THE earliest measurements of gamma-rays emitted upon neutron capture[1,2] were severely limited by the low intensities of natural sources, permitting only a rough estimation of the capture gamma-energies. With the higher fluxes obtainable from the D−D reaction, Kikuchi, Husimi, and Aoki[3] were able to determine capture gamma-energies from an end-point measurement. They were also able to make some estimates of the relative cross sections for gamma-excitation.

The greater fluxes available with the Argonne heavy water pile again made the study of capture gamma-rays expedient.[4] Higher intensities permit study of weak absorbers, and collimated neutron beams provide better geometry than was previously available.

The number of capture gammas emitted is a measure of the total radiation cross section $\sigma(n,\gamma)$, abbreviated in the following as σ_γ. Our experiments measured their intensity by observing the number of Compton electrons which they produced in an aluminum radiator, and the maximum energies of the gamma-rays were measured by the absorption method. Also, the geometry was good enough to permit discernment of the general features of the spectrum of capture gammas emitted.

Figure 1 shows the geometry used for detecting gamma-rays. The unmoderated neutron beam was incident on the target at 15° to the surface to give a large effective target thickness with a minimum multiple scattering. Capture gamma-rays produced at the target passed through a thick boron absorber before striking the aluminum radiator. Neutrons which were scattered off the target were prevented from entering the cylindrical shield directly by this 1-in. absorber, which had the constitution:

B^{10}: 2.16 g/cm²; B^{11}: 0.15 g/cm²; S: 0.96 g/cm².

The aluminum walls of the Geiger counters were 4.6 mils thick. These counters were used both singly and in coincidence; they resolved accidental coincidences separated by more than a microsecond. Irradiations were monitored by a fission counter mounted fully above the beam at the wall of the pile.

QUANTUM ENERGY MEASUREMENTS

Except for the light elements, the energy liberated on neutron capture is 6–10 Mev. This energy may be emitted in a single photon, or there may be a cascade involving several quanta of lower energy. The distribution of quanta among the various possible schemes of decay has been studied only very little. Some theoretical arguments, based on considerations of statistics, would indicate that the maximum energy is rarely, if ever, concentrated in a single quantum. If that were so, a measurement of the maximum energy in the spectrum would yield an energy considerably less than 6–10 Mev.

Previous measurements have been indecisive on this point because of the low intensities of, and the high backgrounds associated with, the sources. The energies which Kikuchi, Husimi, and Aoki found by the end-point method lay between 4 and 7 Mev. Although these values are undoubtedly low, they are, in general, greater than the corresponding values obtained through half-thickness measurements by Rasetti and by Fleischmann.

The technique of the present measurement corresponds closely to the measurements mentioned above for measuring gamma-ray energies by the method of the range of the recoils; successively thicker absorbers are interposed between the two G-M counters, and the thickness of absorber which would eliminate the coincidences altogether gives the energy of the hardest Compton electron.

All absorption curves show a steep decrease, breaking over abruptly into a tail of lesser slope. Our interpretation of the latter effect is that fictitious coincidences not associated with energetic gamma-rays or electrons may be generated in at least two ways: (a) A single gamma-ray may produce Compton electrons in both counters. (b) Brehmsstrahlung from a weak electron in the first counter may fire the second. In either case, the hard component is composed of soft gamma-rays and not hard electrons. The observed absorption coefficients for this component are consistent with gamma-rays of

[1] F. Rasetti, Zeits. f. Physik, **97**, 64 (1935).
[2] R. Fleischmann, Zeits. f. Physik, **103**, 113 (1936).
[3] Kikuchi, Husimi, and Aoki, Proc. Phys. Math. Soc. Japan **18**, 188 (1936).
[4] Such studies of gamma-rays from iron and cadmium were made by H. Lichtenberger using a beam from the original graphite pile, but because of the low intensities the results were only preliminary.

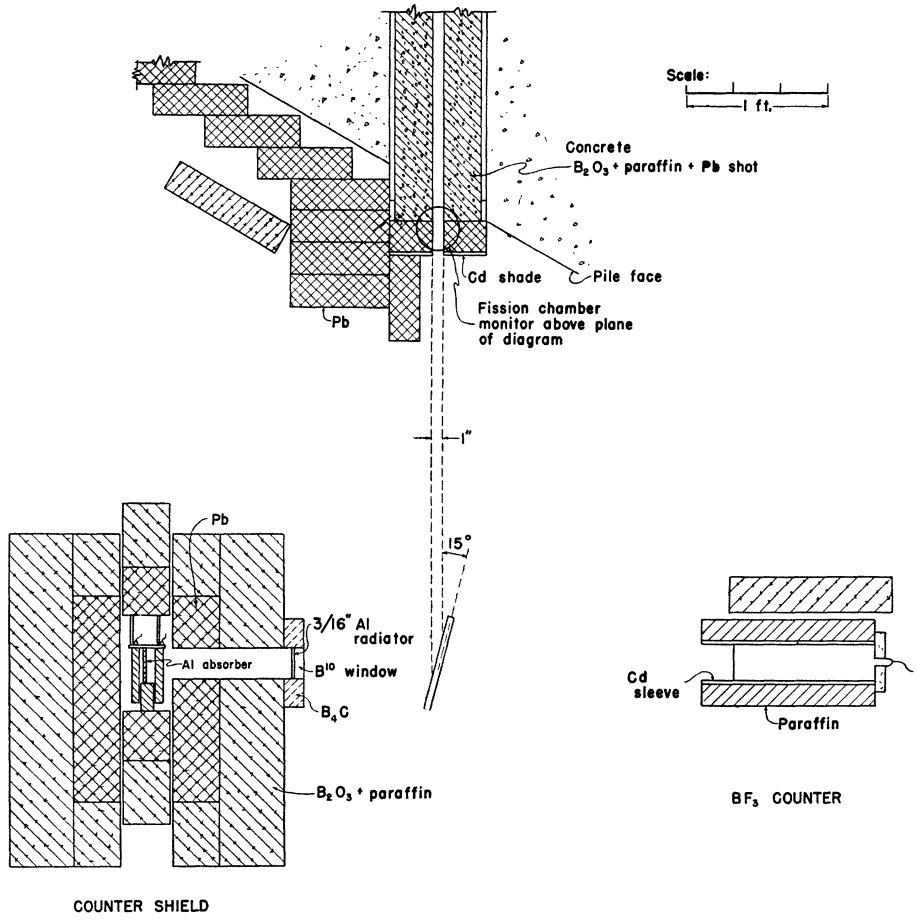

FIG. 1. Geometry for detecting capture γ-rays.

several hundred kev energy, although there is a rather large variation in this absorption coefficient among the various cases. Since in all cases the second component appears to be exponentially absorbed, the procedure has been to extrapolate it exponentially toward zero thickness, then subtract it from the total counting rate. The resultant curve is associated with the desired secondary radiation.

When the end point has been determined, there is added to it the thickness of two counter walls and the air between them (0.07 g/cm^2). From the range so determined, the gamma-ray energy is obtained using the formula $R=0.46E$, where R is the range in Al in g/cm^2, and E is the gamma-ray energy in Mev. This formula fits, within experimental error, the data of Curran, Dee, and Petrzilka,[5] obtained over the range 2–17 Mev by a method similar to the one employed in this experiment.

For each absorber thickness, a subtraction of background must be made. Backgrounds are taken by interposing in the beam an enriched boron plug (approximately 2 g/cm^2 B^{10}) which stops the neutron beam but passes practically all the pile gamma-rays whose effect on the system is part of the background. Also, there is a

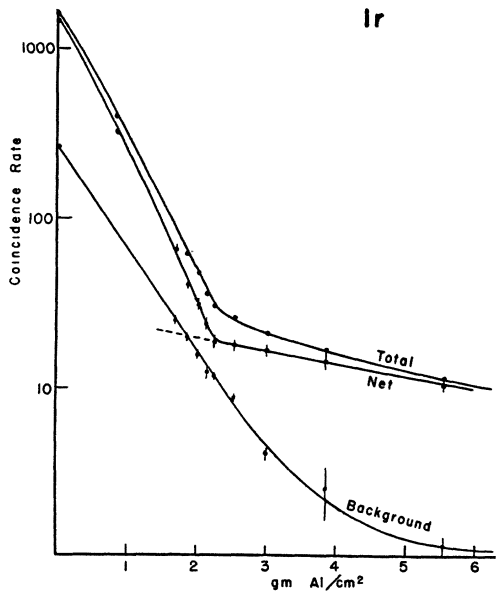

FIG. 2. Detailed absorption curve for the case of iridium. The upper curve indicates total counting rates with the iridium target in place, the lowest curve the measured background rate. The abscissa does not include counter wall thicknesses.

[5] Curran, Dee, and Petrzilka, Proc. Roy. Soc. **169**, 287 (1938).

TABLE I. Maximum energies of capture gamma-rays.

Target	Corrected range (g/cm² Al)	Gamma-ray energy (Mev)	Neutron binding energy	Probable capturing nucleus
S	3.50±0.2	7.6 ±0.4	9.1±0.9	(S^{32})
Cl	4.49±0.2	9.8 ±0.4	8.2±0.95	(Cl^{35})
K	3.32±0.2	7.2 ±0.4	7.1±0.9	(K^{39})
Mn	4.10±0.2	8.9 ±0.4	(7.0)	(Mn^{55})
Fe	3.60±0.3	7.8 ±0.7	8.3±1.6	(Fe^{56})
Co	3.52±0.1	7.7 ±0.2	(7.4)	(Co^{59})
Cu	3.52±0.2	7.7 ±0.4	(7.8)	(Cu^{63})
Ag	3.00±0.35	6.5 ±0.7	(6.9)	(Ag^{109})
Cd	3.22±0.1	7.0 ±0.2	(8.5)	(Cd^{113})
I	3.20±0.2	7.0 ±0.4	(6.2)	(I^{127})
Sm	3.03±0.15	6.6 ±0.3	(7.8)	(Sm^{149})
Gd	2.90±0.2	6.3 ±0.4	(8.6)	(Gd^{157})
W	3.27±0.2	7.1 ±0.3	(6.9)	(W^{186})
Ir	2.37±0.1	5.15±0.2	(6.1)	(Ir^{191})
Au	3.37±0.2	7.3 ±0.4	(6.9)	(Au^{197})
Hg	3.28±0.2	7.1 ±0.4	(6.6)	(Hg^{199})

negligible contribution due to the capture of neutrons in the Al target holder. Figure 2 shows a typical absorption curve, for the case of iridium, with subtraction of background detailed.

Table I summarizes the results as regards maximum gamma-ray energy. The second column gives the secondary electron end point plus 0.07 g/cm². The third column gives the gamma-ray energy derived from this. Estimated probable errors are given. These errors arise chiefly in the subtraction of the exponential tail.

The last column gives independent estimates of the neutron binding energies in the isotope assumed to do the capturing. For four elements (S, Cl, K, Fe) the relevant masses are sufficiently well known to permit the assignment of probable errors. In the remaining cases, the use of a semi-empirical mass formula must be resorted to. Such values, enclosed in brackets, were calculated from[6]

$$M(A,Z)+n-M(A+1,Z)$$
$$=0.01504+0.014[A^{\frac{2}{3}}-(A+1)^{\frac{2}{3}}]$$
$$+0.083\left[\frac{(A/2-Z)^2}{A}-\frac{((A+1)/2-Z)^2}{A+1}\right]$$
$$+0.000627Z^2[A^{-\frac{1}{3}}-(A+1)^{-\frac{1}{3}}]+\delta,$$

where

$$\delta=\mp 0.036A^{-\frac{3}{4}}; \qquad A \text{ even}\begin{cases}Z \text{ even}\\ Z \text{ odd}\end{cases}$$
$$=\pm 0.036(A+1)^{-\frac{3}{4}}; \quad A \text{ odd}\begin{cases}Z \text{ even}\\ Z \text{ odd}\end{cases}$$

and A is the mass number, Z the atomic number.

The maximum gamma-ray energies found in this experiment do not, on the whole, seem to be lower than the estimated neutron binding energies. In fact, considering the uncertainty attached to the two quantities being compared, one is tempted to say that they are identical. If this point of view is substantiated it will make possible the determination of mass differences in many cases where no other technique is available.

A comparison has also been made with the semi-empirical theory of Feenberg.[7] In this formulation, the neutron binding energy is written as $(Q_1+Q_2+Q_3)$. Q_1 is the binding energy that would exist for the nucleus of most stable Z for a given A, (Z_A^*), when even-odd differences are neglected. A plot of Q_1, taken from Feenberg's paper, appears in Fig. 3. Q_2 takes account of the displacement of Z from its optimum value:

$$Q_2=(80/A)(Z-Z^*_{A+\frac{1}{2}})\ \text{m}\mu.$$

Q_3 is a quantity similar to δ, in the Bohr-Wheeler formulation, but slightly different in numerical values.

From the measured gamma-ray energies, E_γ, and from the calculated values of Q_2 and Q_3, we obtain the quantity $(E_\gamma-Q_2-Q_3)$ which should be equal to Q_1 if E_γ is the same as the binding energy, and if the Feenberg theory is correct. The values obtained in this way are shown as the circled points in Fig. 3.

For comparison, we also plot values of $(E_\gamma-Q_2-Q_3)$ obtained in an analogous way from measurements of photo-neutron thresholds with the 22-Mev betatron.[8] All of the previous considerations apply if by A we now mean the atomic weight of the product nucleus. Such points are indicated by triangles.

Considering the experimental errors, the over-all agreement is not unreasonable, but there are several cases where the discrepancies are fairly marked, notably Fe^{53} and Mo^{93} on the high side, as well as Cd^{113}, Sm^{149}, Gd^{157}, and Ir^{191} on the low side. It is probably the case that considerations based on shell structure will be necessary to give a detailed account of neutron binding energies throughout the table.

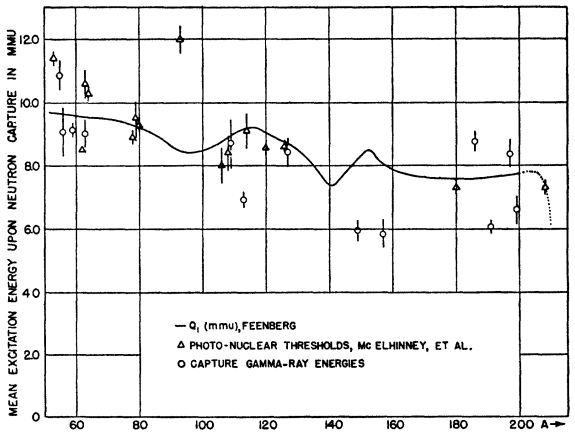

FIG. 3.

[6] N. Bohr and J. A. Wheeler, Phys. Rev. **56**, 426 (1939); G. B. von Albada, Astrophys. J. **105**, 393 (1947).

[7] E. Feenberg, Rev. Mod. Phys. **19**, 239 (1947).

[8] McElhinney, Hanson, Becker, Duffield, and Diven, Phys. Rev. **75**, 542 (1949).

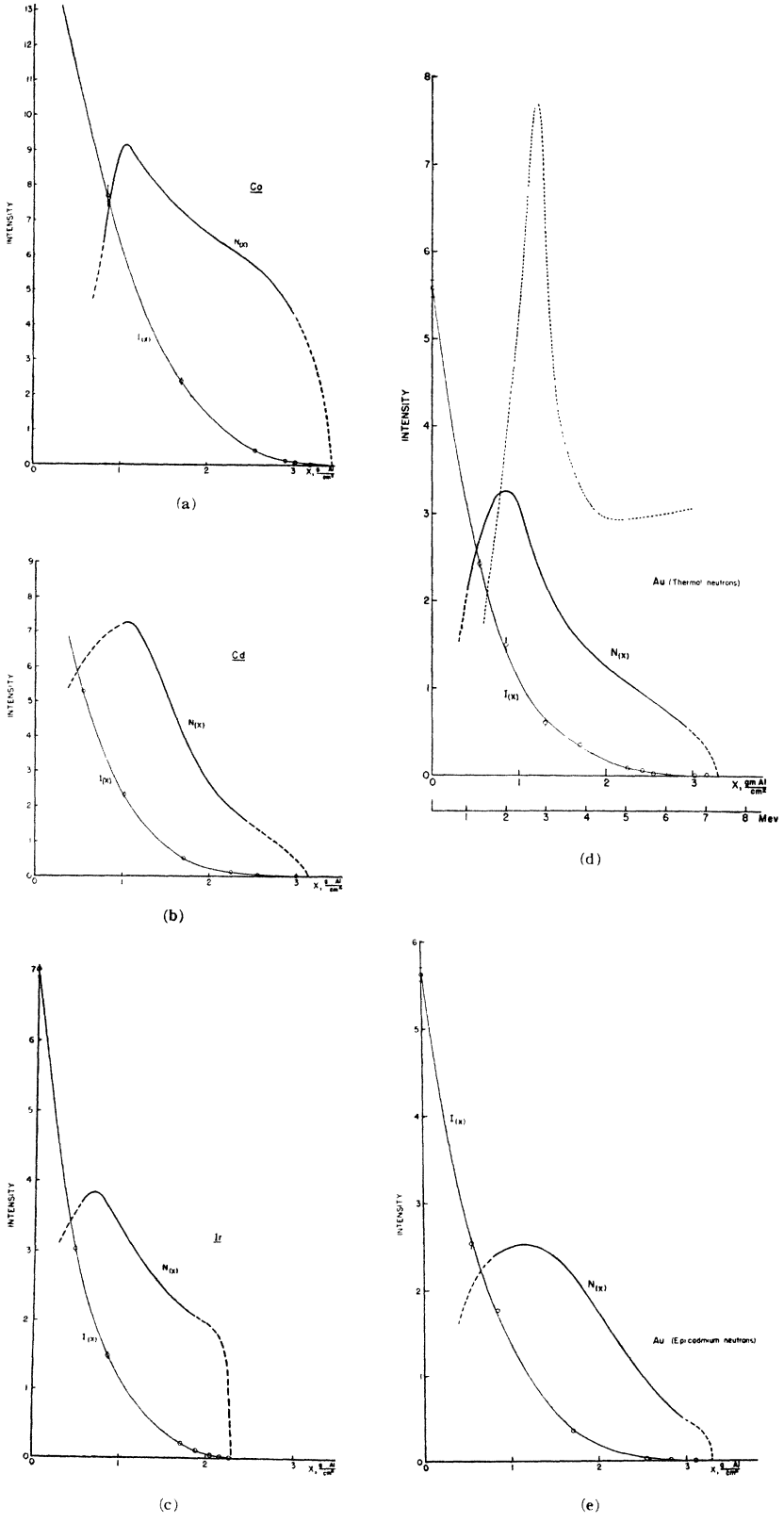

FIG. 4. Absorption curves $I(x)$ and spectral distributions $N(x)$ of capture gamma-rays assuming a sharp range. The dotted curve in Fig. 4(d) represents the spectral distribution on the assumption of linear absorption of secondary electrons.

SPECTRUM OF CAPTURE GAMMAS

The absorption method will, in principle, give some information as to the spectrum of gamma-rays emitted on neutron capture. The following analysis is based on idealized conditions only partially realized in our set-up.

For "high" geometry, the Compton recoils reaching the absorber and counters from the radiator will have been ejected in the forward direction. Let k be the gamma-ray momentum, measured in units mc, where m is the electronic mass. The corresponding range in g/cm² is $R(k)$. If $N(k)dk$ is the number of gamma-ray lines per capture within dk, then the number of electrons incident on the front face of the absorber is

$$I(0)=\int_0^\infty dkCN(k)\phi(k)R(k),$$

where $\phi(k)$ is the differential cross section for Compton scattering in the forward direction and C is a constant of the apparatus. As absorber is added the contribution of any particular k to the integral decreases linearly until absorber of amount $R(k)$ is reached. Hence, at absorber thickness x g/cm²,

$$I(x)=\int_{k_{\min}}^\infty dkCN(k)\phi(k)R(k)[1-x/R(k)]. \quad (1)$$

The lower limit is determined by $R(k_{\min})=x$.

Since $k_{\min}$ is a function of x,

$$d^2I/dx^2=CN(k_m)\phi(k_m)(dk_m/dx)$$

or, suppressing the subscript,

$$N(k)=[(d^2I/dx^2)]/[C\phi(k)(dk/dx)],$$

where $R(k)=x$. Experimentally we know that (dk/dx) is essentially constant in the range under consideration (1−8 Mev). $\phi(k)$ is obtained from the Klein-Nishina formula and is proportional to

$$\frac{1}{k+\frac{1}{2}}\left[1+\frac{1}{4(k+\frac{1}{2})^2}\right].$$

Using the formula previously quoted for the relation between energy and range, this becomes

$$N(k)=C'(x+0.118)[1+0.25(x+0.118)^{-2}]^{-1}d^2I/dx^2. \quad (2)$$

Formula (2) will be limited in its application because of the fact that electrons, particularly of low energy, do not have a sharp range. The effect of this will be to introduce a finite resolution to the spectral analysis. The resolution width will be that interval of k corresponding to the range straggling.

Other limitations are due to the non-exclusion of some recoils which must have originated elsewhere than in the radiator, and the contribution from pair electrons. These effects can be shown to be unimportant, to the accuracy of our analysis. The contributions from photo-electrons in this experiment were entirely negligible since the counter walls and air between them stopped all electrons below 0.15 Mev.

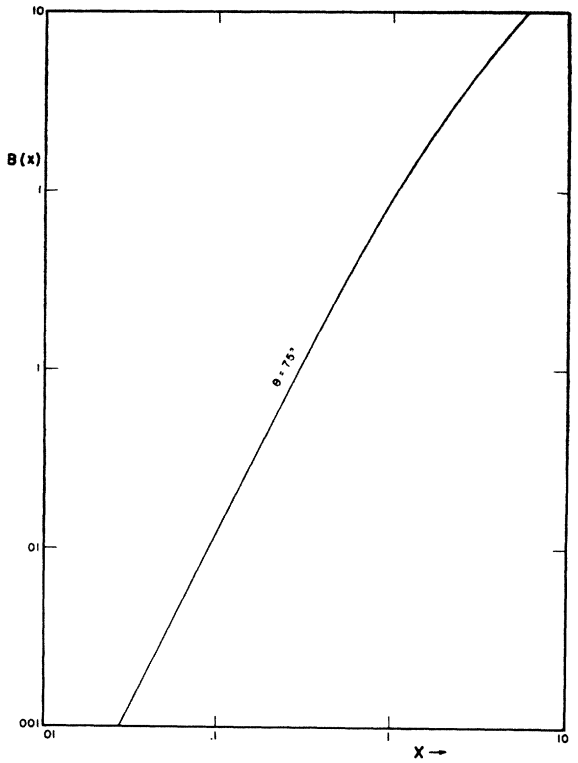

FIG. 5. $B(x)$ for $\theta=75°$.

Finally, the data must be very accurate and complete in order that the curve may be subjected to two differentiations with assurance. Only in a few cases did we consider the application of this method justified, and there only for distinguishing outstanding features of the spectral distribution. These absorption curves for the elements Cd, Ir, Au, and Co with their calculated distributions are shown in Fig. 4.

Within the above limitations we note that these elements have maxima between 1.5 Mev and 2.5 Mev. The positions of these maxima agree with those predicted by Bethe for the radiation emitted in the capture process itself.[9] Bethe's theory is based on the statistical theory of energy level density and on the assumption that the dipole moments for all possible transitions are of the same order. Because of the rapid increase of level density with energy on this model, transitions from the capture level all the way to the ground level (or nearly all the way) are highly improbable as compared to transitions of about a third that energy. This implies that the distribution curves $N(x)$ in Fig. 4 should show a high order of contact at the upper energy limit. However, the experimental distributions, in fact, show many quanta near the maximum energy. Thus, the

[9] H. A. Bethe, Rev. Mod. Phys. 9, 233 (1937).

TABLE II. Summary of experimental results.

Target	g/cm²	$\langle A\phi\rangle_{Av}$	σ_r	σ_t	G_s/G_θ	Y	Δ%
			I. Very strong absorbers				
Rh	0.1115	0.243	110	115		1.13	4
Ag	0.0424	0.945	45	50		1.05	4
Cd	0.0222	0.055	2260	2266	All	1.41	3
Cd	0.01537	0.055	2260	2266	less	1.39	3
In	0.0229	0.89	140	145	than	0.96	4
Ir	1.092	0.062	300	300	0.001	0.89	4
Au	0.2632	0.246	72	78		0.993	3
Au	0.2632	0.246	72	78		0.992	3
Au	0.0566	0.89	72	78		1.010	3
Hg	0.2411	0.246	370	370		1.08	3
			II. Strong absorbers				
$C_{1/3}Cl$	0.591	0.055	25	30	0.020	1.46	8
Mn	0.532	0.246	9.4	11.9	0.011	1.23	4
Co	0.470	0.194	25	30	0.009	1.32	4
Ta	0.398	0.166	19	24	0.029	0.73	5
W	0.236	0.945	10	17.5	0.029	1.16	4
Pt	0.494	0.246	8.1	16.1	0.001	1.19	5
			III. Weak absorbers				
Mg	0.574	1.0	0.30	3.2	0.53	0.47	12
Al	0.850	1.06	0.17	1.6	0.19	1.05	11
S	0.726	0.246	0.4	1.9	0.09	1.52	7
Fe	0.474	1.06	1.9	12.9	0.15	1.53	7
Fe	0.989	0.246	1.9	12.9	0.18	1.53	7
Ni	0.709	0.246	3.3	18.8	0.12	1.86	6
Cu	1.50	0.246	3.0	10.8	0.08	1.34	5
Cb	0.0974	0.591	1.3	6.3	0.17	1.18	17
Sn	0.233	1.06	0.49	5.49	0.23	1.26	7
			IV. Very weak absorbers				
Pb	3.65	1.06	0.13	11.1	0.73	1.46	16

assumptions mentioned above are thrown seriously in doubt.

We could carry out an alternative analysis assuming that monokinetic electrons, instead of showing a sharp range, decrease linearly in penetrating the absorber. This assumption is known to describe fairly well the absorption of electrons of energy about 1 Mev. In the energy range being studied, the absorption would be intermediate in character between these two cases.

With the assumption of linear absorption, it is necessary to carry out three differentiations to obtain a spectral distribution. In general, the result is to emphasize the high energy end, moving the maximum slightly toward higher energies and strongly intensifying the number of quanta near the high energy limit (by about a factor of two compared to the number in the peak). The dotted curve in Fig. 4(d) gives this alternative distribution as derived from the data for Au.

While it is clear that quantitative conclusions regarding the spectral distribution can hardly be obtained, it is also clear that the number of high energy quanta present is far greater than the statistical theory of nuclear energy levels would predict.

Absorption curves for gold were made using thermal and epi-cadmium neutrons, respectively, and are shown in Figs. 4(d) and 4(e). Within experimental error the curves have the same shape and the same end point. The evidence is, therefore, that the decay of radioactive gold nuclei formed in the 5-ev resonance level involves the same radiative processes as for those gold nuclei formed by capture of thermal neutrons.

GAMMA-RAY YIELD MEASUREMENTS

Gamma-ray yield measurements were made in a survey of targets of a number of materials. A beam of neutrons of energy below the cadmium cut-off (hereafter called *thermal* for convenience) was permitted to fall on each target and the corresponding counting rates were observed in the Geiger counters inside the shield. These rates were compared with the rates of neutron capture calculated for the various targets from tabulated neutron cross sections. The ratio thus obtained is, as will be shown, approximately proportional to the total number of gamma-rays emitted on neutron capture. The constancy of this ratio would indicate a similarity in the spectra of capture gamma-rays for the various targets. However, some deviation from constancy is to be expected because of the variation of neutron binding energy among the substances studied.

For each target the following measurements were taken both with Geiger-Müller counters and with a boron trifluoride counter located directly adverse to the G-M counters and in a standard position about three feet from the target.

N_1: counting rate with the sample in open beam; sample mounted on and behind a thin aluminum holder,
N_2: holder alone in open beam,
N_3: sample in beam blocked off with Cd filter,
N_4: holder in Cd-filtered beam.

For thermal neutrons the significant rate for the G-M counters is

$$G_\theta=(N_1-N_2)-(N_3-N_4) \tag{3}$$

and may be compared with a calculated number

$$K=K_i+K_d+K_s. \tag{4}$$

K_i is the number of neutrons captured from the beam on first traversal of the target. K_d is the number of additional captures in the sample for neutrons scattered on first traversal, and is of significance only when the substance is such a weak absorber that a considerable thickness is necessary for counting. K_s is a contribution arising from neutrons scattered by the target which are subsequently captured in or near the shield producing detectable gamma-radiation. This contributes a fictitious absorption cross section and is dominant for a weak absorber such as graphite.

If a beam with flux ϕ falls on a target at an angle θ with the normal, then the rate of initial radiative capture is

$$K_i=A\phi\cos\theta(\sigma_r/\sigma_t)(1-\exp(-Nl\sigma_t\sec\theta)), \tag{5}$$

where N is the number of atoms/cm³, l is the thickness in cm, σ_r is the radiative capture cross section, σ_t the total cross section, and A the area of the sample.

Furthermore, the secondary term K_d becomes for samples thin compared with a diffusion length (a valid approximation for all our samples),

$$K_d = A\phi \cos\theta[\kappa^2/(\nu^2-\kappa^2)]B(\nu), \quad (6)$$

where

$$\nu = N\sigma_t \sec\theta; \quad \kappa = N(3\sigma_r\sigma_t)^{\frac{1}{2}}(1-0.42\sigma_r/\sigma_t),$$
$$B(x) = (1-e^{-x})(0.71\times\sec.\theta-1)+x/2(1+e^{-x}).$$

A plot of $B(x)$ for $\theta = 75°$ is shown in Fig. 5.

Finally, the number of scattered neutrons leaving the target is $K_s = K_i(\sigma_s/\sigma_r)$ to very good approximation.

We define a yield Y as

$$Y = (G_\theta - G_s)/A\phi(K_i + K_d). \quad (7)$$

G_θ is the net Geiger counting rate, given by (3). G_s is that part of the Geiger counting rate due to neutrons scattered out of the beam by the target; shielding made this term small but not negligible. The numerator of (7) is therefore the counting rate due solely to captures in the target. The denominator is the predicted rate of captures, calculated from tabular cross sections.

The magnitude of the correction G_s was determined in two independent ways,

(A) We may write $G_s = mK_s$, with K_s calculated as above from tabular cross sections. m is a constant of the apparatus which may be determined empirically by using as a target an element whose capture cross section is so small that the observed count in our set-up is due to scattering entirely. Carbon is such an element. Carbon targets of various sizes were used to determine corresponding values of m above for each size and for each counter.

(B) We may also write $G_s = nB_\theta$, where B_θ is the net rate of counting of the BF_3 counter obtained, as in (3), by a difference of four measurements. B_θ is proportional to the actual number of scattered neutrons, hence to G_s, and n is another constant of the apparatus. Bismuth was used as the standard for this measurement. The values of n were found to be 0.200, 0.123, and 0.0394, for the fore singles counter, the rear singles counter, and the coincidences, respectively, for the standard foil. It follows that the effect of scattered neutrons was more important for the near counter than for the far one.

Any serious deviation between the values of G_s as determined by (A) and (B) would imply error either in the BF_3 counting or in the tabular cross sections. In fact, the agreement was reasonably good for almost all the cases. Our final tabulation of yield uses an average G_s, obtained as the average of (A) and (B). Deviation between the two values is taken account of in the probable error. Only in the case of aluminum is this the dominant contributing factor to the probable error.

The measurement of $\langle A\phi\rangle_{Av}$, the integrated neutron flux striking the target, was made by cutting Cd and brass dummies of the same areas as the various targets (which varied in size from a circle 1 in. in diameter for Cd to a rectangle $5\frac{1}{2}$ in.$\times$11 in. for Pb) and inserting these into the neutron beam. The highly emissive Cd dummy targets could be counted only with the pile operating at reduced intensity. These values of $\langle A\phi\rangle_{Av}$ were then referred to a standard value of unity for 4-in.$\times$9-in. targets, and are recorded in Table II in the appropriate column.

EXPERIMENTAL RESULTS

Table II summarizes the experimental results. The elements are divided into four groups according to the ascending importance of the scattering contribution G_s. However, this contribution is predominant in the last group only. The term K_d is negligible compared to K_i over most of the table, reaching a value about 10 percent of K_i only in the last group. The columns indicate the following:

Target: the element or compound used, normalized to one atom of the capturing element.
$\langle A\phi\rangle_{Av}$: the relative neutron flux intercepted by the target.
σ_r: the radiative capture cross section in barns, essentially taken from Table 9.5 of *The Science and Engineering of Nuclear Power*, Coryell, *et al.* (Addison-Wesley, 1947), and corrected to an assumed Maxwellian distribution at 400°K.
σ_t: tabular cross section in barns from the above table.
(G_s/G_θ): the fractional Geiger counting rate due to neutrons scattered out of target (average of two independent methods of determination).
Y: relative gamma-ray yield. This is the yield defined by (7), but referred for convenience to gold as having the value unity. Included here are the data from the fore singles counter, the rear singles counter, and the coincidence circuit; the yield as measured by each is divided by the corresponding one for gold and the three resulting numbers averaged with the coincidence data given half-weight.
Δ: the probable error in the relative gamma-ray yield.

DISCUSSION

With a few exceptions, the yields occupy the range of 0.9 to 1.6. That is to say, the variation about the mean is ± 30 percent; the chosen standard, gold, seems to have a yield considerably below the mean.

No marked correlations of yield with other parameters seem evident. Extreme cases are magnesium with a yield of 0.47 and nickel with 1.86.

Referring to the previous analysis and reasoning leading to Eq. (1), we see that the yield measured by this experiment is, to a fair approximation, proportional to the total number of gamma-rays emitted on neutron capture. In the expression for $I(0)$, the product $R(k)\phi(k)$ is about constant, and the quantity being measured becomes proportional to $\int dkN(k)$. This conclusion is independent of any special assumption as to the fashion in which the secondary electrons are absorbed.